

Supporting information

Rhodamine-Naphthalimide Demonstrated a Distinct Aggregation-Induced Emission Mechanism: Elimination of Dark-States via Dimer Interactions (EDDI)

Qingkai Qi,^a Lu Huang,^{b,c} Runqing Yang,^d Jin Li,^a Qinglong Qiao,^a Bin Xu,^d Wenjing Tian,^{*d} Xiaogang Liu^{*b} and Zhaochao Xu^{*a}

^aCAS Key Laboratory of Separation Science for Analytical Chemistry, Dalian Institute of Chemical Physics, Chinese Academy of Sciences, Dalian 116023, China.

^bSingapore University of Technology and Design, 8 Somapah Road, Singapore 487372, Singapore.

^cMinjiang University, Fuzhou 350108, China.

^dState Key Laboratory of Supramolecular Structure and Materials, Jilin University, Changchun 130012, China.

* Email: zcxu@dicp.ac.cn, xiaogang_liu@sutd.edu.sg, wjtian@jlu.edu.cn

Table of Contents

1. General information for synthesis and characterizations.
2. Summary of photophysical parameters of RhB-Naph and reference compound Naph.
3. PL spectra of RhB-Naph and Naph in THF and water mixture with different water fraction.
4. UV-vis absorption and PL spectra of RhB-Naph in CH₂Cl₂ before and after adding CF₃COOH.
5. PL excitation spectra of molecular aggregates of RhB-Naph in THF-water mixture.
6. Fluorescence lifetime of molecular aggregates of RhB-Naph in THF-water mixture and RhB in THF solution.
7. UV-vis absorption and PL spectra of RhB-Naph in THF solution at different concentration.
8. PL spectra of RhB-Naph in ethanol-glycerol mixture with different glycerol fraction.
9. Crystal data, intensity collection parameters and ORTEP drawing of RhB-Naph.
10. Dihedral angles between xanthene, naphthalimide and isoindolin-1-one moieties in RhB-Naph monomer and dimer.
11. Vertical excitation energies to various singlet excited states, optimized molecular structure, HOMO and LUMO and of Naph in dichloromethane.
12. Phosphorescence spectra of frozen solution of RhB-Naph in different solvent.
13. PXRD pattern of the pristine powder and the simulated PXRD pattern delineated on the basis of the crystal structure using the single crystal software Mercury 3.10.1.
14. Fluorescent lifetimes of RhB-Naph powders after different treatments.
15. ¹HNMR, ¹³CNMR and HRMS spectra of the compounds.
16. References.

1. General information for synthesis and characterizations.

Materials

Rhodamine B (RhB), butylamine, phosphorus oxychloride, 1,2-dichloroethane, chloroacetyl chloride and trimethylamine were purchased from Energy Chemical and used as received. 4-amino-1,8-Naphthalic anhydride was synthesized according to previous literature report.¹ The solvent and all the other chemicals were purchased from Aladdin and used as received without further purification.

Instruments

¹H NMR spectra were recorded on a 400 MHz BrukerAvance, using CDCl₃ or DMSO-*d*₆ as solvent and tetramethylsilane (TMS) as an internal standard ($\delta = 0.00$ ppm). ¹³C NMR spectra were recorded on a 101 MHz BrukerAvance, using CDCl₃ as a solvent and CDCl₃ as an internal standard ($\delta = 77.00$ ppm). Mass spectrometry data were obtained with a HP1100LC/MSD mass spectrometer. UV-vis absorption spectra were collected on an Agilent Cary 60. Fluorescence spectra were recorded by Shimadzu RF-5301 PC spectrometer and Maya2000Pro optical fiber spectrophotometer. Solid state PL efficiencies were measured using an integrating sphere (C-701, Labsphere Inc.), with a 365 nm Ocean Optics LLS-LED as the excitation source, and the light was introduced into the integrating sphere through optical fiber. The powder X-ray diffraction patterns were recorded by Rigaku SmartLab X-ray diffractometer with Cu K α radiation ($\lambda = 1.5418$ Å) at 25 °C (scan range: 5-50°). Fluorescence Lifetimes were performed using time-correlated single-photon counting (TCSPC) method and collected on an Edinburgh FLS980, with an Edinburgh EPL-375 picosecond pulsed diode laser as the excitation source.

Computational method

Density functional theory (DFT) and time-dependent (TD)-DFT calculations were performed using *Gaussian 16*.² Geometry optimizations employed the M062X functional³, in combination with the def2SVP basis set. When applicable, solvent effects (dichloromethane) were considered using the SMD model⁴. Frequency checks were carried out after each geometry optimization to ensure that the minima on the potential energy surfaces (PES) were found. Based on the optimized structure, we also computed the vertical excitation energies to various singlet and triplet states using TD-DFT with the linear solvation formalism.

Single-crystal structure

Single crystal of **RhB-Naph** was obtained by slow evaporation from the chloroform/n-hexane solution at room temperature. Single crystal X-ray diffraction data were collected on a Xcalibur, Atlas, Gemini ultra-diffractometer using the ω -scan mode with graphite-

monochromator Mo K α radiation. The crystal structure was solved with the Superflip⁵ structure solution program and refined with the SHELXL⁶ refinement package, as implemented in OLEX2⁷. These data can be obtained free of charge from the Cambridge Crystallographic Data Centre (CCDC reference numbers: 1858079).

Synthesis and characterizations

Synthesis of 4-Amino-9-(*n*-butyl)-1,8-Naphthalimide: 4-Amino-9-(*n*-butyl)-1,8-Naphthalimide was synthesized according to previous literature reports.⁸ ¹H NMR (400 MHz, DMSO) δ 8.61 (d, J = 8.4 Hz, 1H), 8.43 (d, J = 7.2 Hz, 1H), 8.20 (d, J = 8.3 Hz, 1H), 7.66 (t, J = 7.8 Hz, 1H), 7.41 (s, 2H), 6.85 (d, J = 8.4 Hz, 1H), 4.01 (t, J = 7.3 Hz, 2H), 1.65 – 1.51 (m, 2H), 1.34 (dd, J = 14.8, 7.4 Hz, 2H), 0.92 (t, J = 7.3 Hz, 3H).

Synthesis of Naph: **Naph**, as a model compound, was synthesized as shown in Scheme 1. To a solution of 4-Amino-9-(*n*-butyl)-1,8-Naphthalimide (200 mg, 0.37 mmol) in 30 mL THF was dropwise added 3-chloropropionyl chloride (473 mg, 3.72 mmol) at 0 °C. After 30 min, the mixture was removed to room temperature and stirred overnight. The solvent was removed by evaporation without further purification. The residue was dissolved in 50 mL acetonitrile and was added K₂CO₃ (154 mg, 1.12 mmol). After stirring for 1 h at 60 °C, the mixture was cooled to room temperature, and the solvent was removed under reduced pressure to obtain white solid, which was purified by column chromatography (silica gel, CH₂Cl₂ : MeOH = 400 : 1) to afford Naph as a white powder (55 mg, 44%). ¹H NMR (400 MHz, CDCl₃) δ 8.62 (s, 1H), 8.60 (d, J = 2.7 Hz, 1H), 8.13 (d, J = 8.4 Hz, 1H), 7.76 (t, J = 7.9 Hz, 1H), 7.62 (d, J = 7.8 Hz, 1H), 4.26 – 4.10 (m, 1H), 3.99 (t, J = 6.9 Hz, 1H), 2.75 (t, J = 8.0 Hz, 1H), 2.47 – 2.32 (m, 1H), 1.71 (dt, J = 15.2, 7.6 Hz, 1H), 1.44 (dq, J = 14.7, 7.3 Hz, 1H), 0.98 (t, J = 7.3 Hz, 1H). LC-MS (ESI): m/z : calcd: 336.1474; found: 337.1546 [M+H]⁺. Elemental analysis calcd (%) for C₂₀H₂₀N₂O₃: C 71.41, H 5.99, N 8.33, O 14.27; found: C 72.02, H 6.05, N 8.38, O 14.60.

Synthesis of RhB-Naph: **RhB-Naph** was synthesized as shown in Scheme 1. The mixture of RhB (191 mg, 0.4 mmol) and POCl₃ (610 mg, 4 mmol) was refluxed in 1,2-dichloroethane (15 mL) for 2 h, after which the solvent was removed to give dark violet-red oil. The crude acid chloride was dissolved in CH₂Cl₂ (15 mL), then trimethylamine (0.3 mL) and 4-Amino-9-(*n*-butyl)-1,8-Naphthalimide (107 mg, 0.4 mmol) were dropwise added into the mixture solution. The reaction mixture was stirred at room temperature for 24 h. Then, the solvent was removed and the crude residue was purified with column chromatography (silica gel, petroleum ether:ethyl acetate = 4:1) to give RhB-Naph as a yellow powder (180 mg, 65%). ¹H NMR (400 MHz, CDCl₃) δ 8.42 (d, J = 6.7 Hz, 1H), 8.29 (d, J = 7.8 Hz, 1H), 8.10 (d, J = 6.8 Hz, 1H), 7.74 – 7.61 (m, 3H), 7.39 (t, J = 7.7 Hz,

2H), 6.72 (t, $J = 8.3$ Hz, 2H), 6.57 (d, $J = 7.8$ Hz, 1H), 6.45 (dd, $J = 8.9, 2.3$ Hz, 1H), 6.29 – 6.18 (m, 2H), 5.87 (d, $J = 2.3$ Hz, 1H), 4.12 (t, $J = 7.5$ Hz, 2H), 3.47 – 3.30 (m, 4H), 3.24 – 3.07 (m, 4H), 1.63 – 1.72 (m, 2H), 1.48 – 1.37 (m, 2H), 1.20 (t, $J = 7.0$ Hz, 6H), 1.05 – 0.92 (m, 9H). ^{13}C NMR (101 MHz, CDCl_3) δ 166.97, 164.21, 163.90, 154.38, 153.63, 151.20, 149.24, 148.85, 139.50, 133.20, 132.10, 130.95, 130.86, 130.64, 129.70, 128.98, 128.82, 128.73, 128.66, 127.58, 126.07, 124.66, 123.75, 122.54, 122.21, 108.37, 107.65, 106.63, 105.91, 97.78, 97.55, 69.54, 44.45, 44.29, 40.17, 30.15, 20.35, 13.81, 12.48, 12.29. LC-MS (ESI): m/z : calcd: 692.3363; found: 693.3453 $[\text{M}+\text{H}]^+$. Elemental analysis calcd (%) for $\text{C}_{44}\text{H}_{44}\text{N}_4\text{O}_4$: C 76.28, H 6.40, N 8.09, O 9.24; found: C 76.35, H 6.52, N 8.10, O 9.40.

2. Summary of photophysical parameters of RhB-Naph and reference compound Naph.

Table S1. Summary of photophysical parameters of **RhB-Naph** and reference compound **Naph**.^a

Compound	$\lambda_{\text{abs,solution}}$ (nm)	$\lambda_{\text{em,solution}}$ (nm)	$\lambda_{\text{em,solid}}$ (nm)	$\Phi_{\text{F,solution}}$ (%)	$\Phi_{\text{F,solid}}$ (%)
RhB-Naph	346, 321	—	518	<0.01	5
Naph	346	438	450	96	43

^aAbbreviations: λ_{abs} = UV-vis absorption maximum, λ_{em} = emission maximum, Φ_{F} = fluorescence quantum yield. Notes: UV-vis absorption and emission peaks were all obtained in their DCM solution. $\Phi_{\text{F,solution}}$ were recorded by using quinine sulfate in 0.1 M H_2SO_4 ($\Phi_{\text{F}} = 0.54$, excitation wavelength of 365 nm). $\Phi_{\text{F,solid}}$ were determined using a calibrated integrating sphere.

3. PL spectra of RhB-Naph and Naph in THF-water mixtures with different water faction.

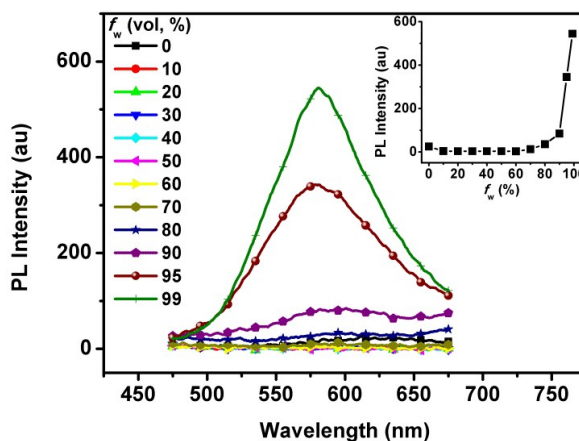


Figure S1. PL spectra of **RhB-Naph** (10^{-5} M) in THF and water mixture with different water fraction (f_w). Inset: plot of PL intensity versus f_w . Excitation wavelength: 365 nm.

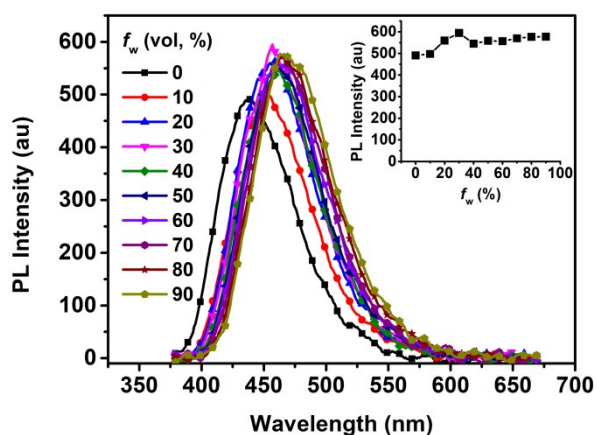


Figure S2. PL spectra of **Naph** (10^{-5} M) in THF-water mixture with different water fraction (f_w). Inset: plot of PL intensity versus f_w . Excitation wavelength: 350 nm.

Notes: We have measured the AIE feature of model compound **Naph** in THF-water mixture with different water fraction (f_w). As can be seen from Figure SX, the model compound **Naph** did not show obvious AIE nor ACQ features. **Naph** emit strong blue fluorescence in both the solution and solid phases ($\Phi_{F,solution} = 96\%$, $\Phi_{F,solid} = 43\%$).

4. UV-vis absorption and PL spectra of RhB-Naph in CH_2Cl_2 before and after adding CF_3COOH .

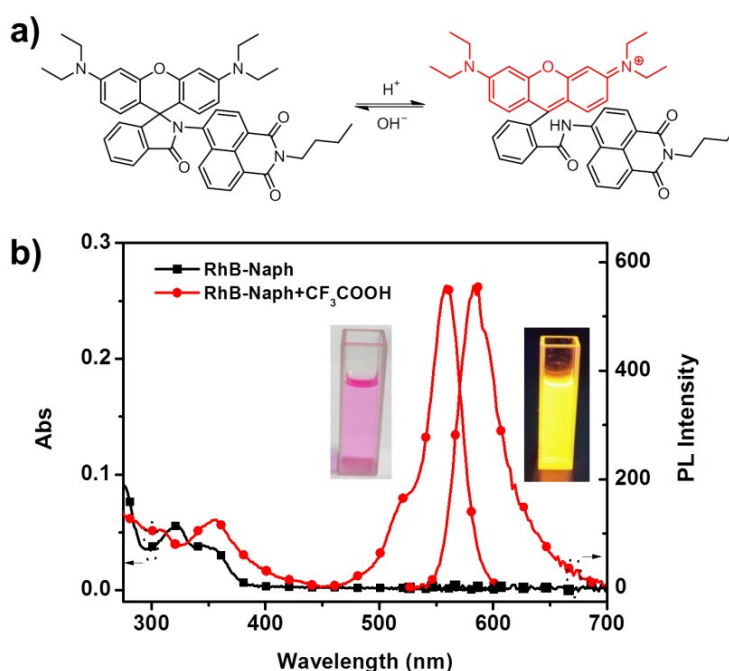


Figure S3. a) Chemical structures switch of **RhB-Naph** under acid/base stimuli. b) UV-vis absorption and PL spectra of **RhB-Naph** in CH_2Cl_2 (10^{-5} M) before and after adding 2.2 μ L CF_3COOH (1000 equiv). Inset: visible and fluorescence images of the solution after adding CF_3COOH . Excitation wavelength: 500 nm.

5. PL excitation spectra of molecular aggregates of RhB-Naph in THF-water mixture.

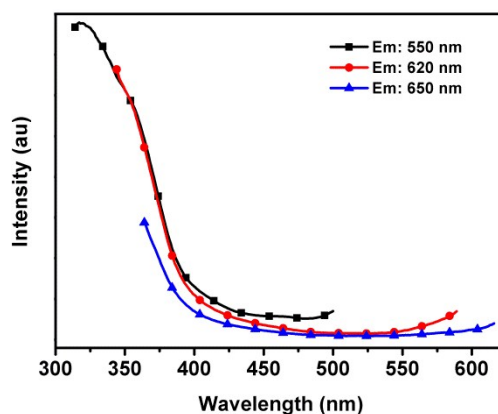


Figure S4. PL excitation spectra of molecular aggregates of **RhB-Naph** formed in THF-water mixture (f_w , 90%) at the different emission wavelength (550/620/650 nm).

Notes: We probed the PL excitation spectra of the observed emissions in THF-water mixture (f_w , 90%). These fluorescence excitation spectra peaked at ~ 320 nm, which is apparently different from the characteristic absorption band of the ring-opened rhodamine at ~ 560 nm (Figure S4).

6. Fluorescence lifetime of molecular aggregates of RhB-Naph in THF-water mixture and RhB in THF solution.

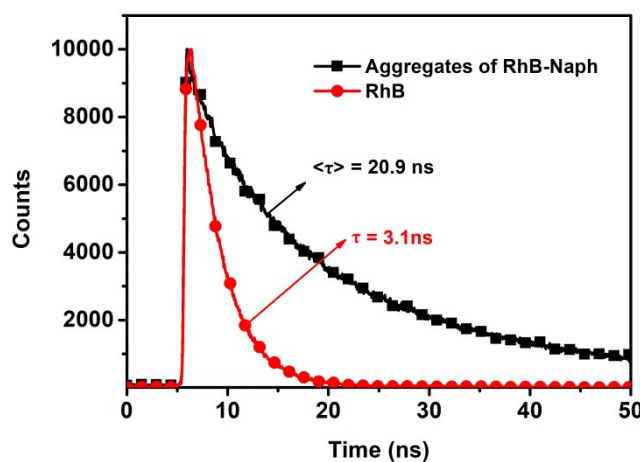


Figure S5. Fluorescent lifetime of **RhB-Naph** aggregates in THF-water mixtures ($f_w = 90\%$) and RhB in THF solution. ($[\text{RhB-Naph}] = 10^{-5}$ M, $[\text{RhB}] = 10^{-5}$ M).

Notes: we compared the emission lifetime of **RhB-Naph** solution, as well as ring-opened **RhB** solution. The lifetime of RhB-Naph (20.9 ns) is significantly longer than that of RhB (3.1 ns).

7. UV-vis absorption and PL spectra of RhB-Naph in THF solution at different concentrations.

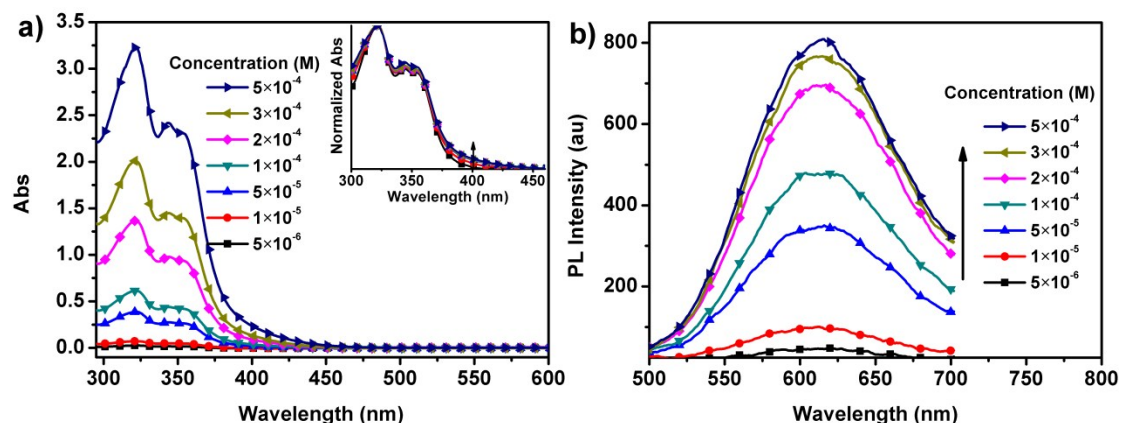


Figure S6. a) UV-vis absorption and b) PL spectra of **RhB-Naph** in THF solution at different concentrations. Inset in a): Normalized UV-vis absorption spectra. Excitation wavelength: 365 nm.

Notes: We have measured the UV-vis absorption and PL spectra of **RhB-Naph** in solution at different concentrations in the revised Supporting Information (Figure S6). The fact that molecular aggregation took place with increased **RhB-Naph** concentrations can be deduced from the lifted spectral tails in UV-vis absorption spectra (Figure S6a), which are caused by light-scattering effects. Besides, the aggregates of **RhB-Naph** formed with obvious turn-on emissions at ~ 600 nm (Figure S6b). The observed emission wavelengths are considerably different from that of the model compound **Naph** (~ 440 nm) and are thus attributed to molecular aggregates of **RhB-Naph**.

8. PL spectra of RhB-Naph in ethanol-glycerol mixture with different glycerol fraction.

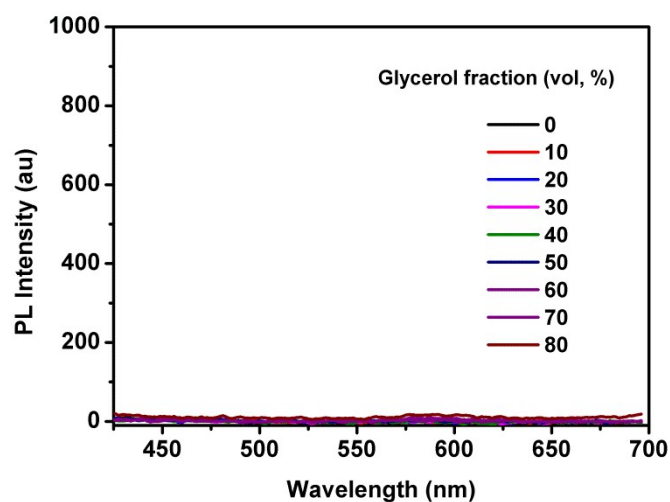


Figure S7. a) PL spectra of **RhB-Naph** (10^{-5} M) in ethanol-glycerol mixture with different glycerol fraction. Excitation wavelength: 365 nm.

9. Crystal data, intensity collection parameters and ORTEP drawing of RhB-Naph.

Table S2. Summary of crystal data and intensity collection parameters of **RhB-Naph**.

Crystal	RhB-Naph
Empirical formula	C ₄₄ H ₄₄ N ₄ O ₄
Formula weight	692.33
Crystal system	Triclinic
Space group	P-1
a, Å	9.9350(8)
b, Å	12.2145(10)
c, Å	15.7216(13)
α , deg	78.776(7)
β , deg	75.149(7)
γ , deg	83.468(7)
Volume, Å ³	1804.7(3)
Z	2
D _x , g/cm ³	1.271
M _{μ} /mm ⁻¹	0.082
F_{000}	680.0
Temp, (K)	293
$M(\text{Mo K}\alpha)$, mm ⁻¹	0.079
2 θ range, deg	5.58-58.78
Reflections collected	18346
Independent reflections	8560
$R(\text{int})$	0.1083
Data/restraints/parameters	8560/0/446
R_1 , w R_2 [obs $I > 2\sigma(I)$]	0.1890, 0.4639
R_1 , w R_2 (all data)	0.3669, 0.5529
Residual peak/hole e. Å ⁻³	1.84/-0.45
Goodness-of-fit on F^2	1.232
CCDC number	1858079

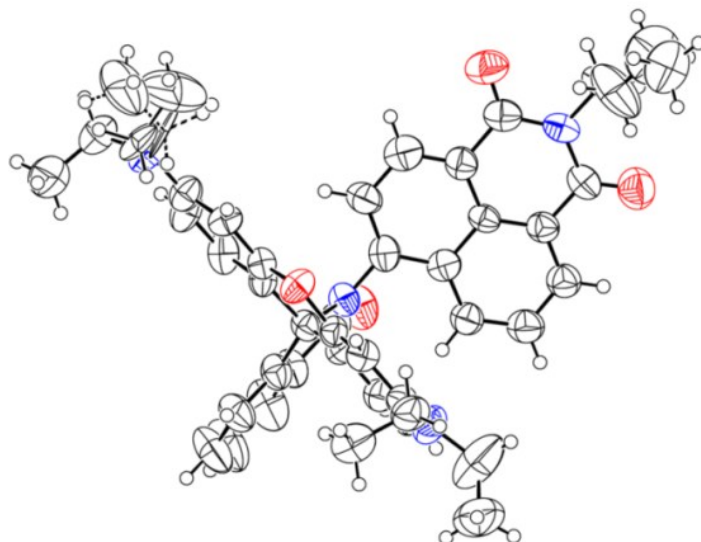


Figure S8. ORTEP drawing (50% probability ellipsoids) of the crystal structure of **RhB-Naph**.

10. Dihedral angles between xanthene, naphthalimide and isoindolin-1-one moieties in RhB-Naph monomer and dimer.

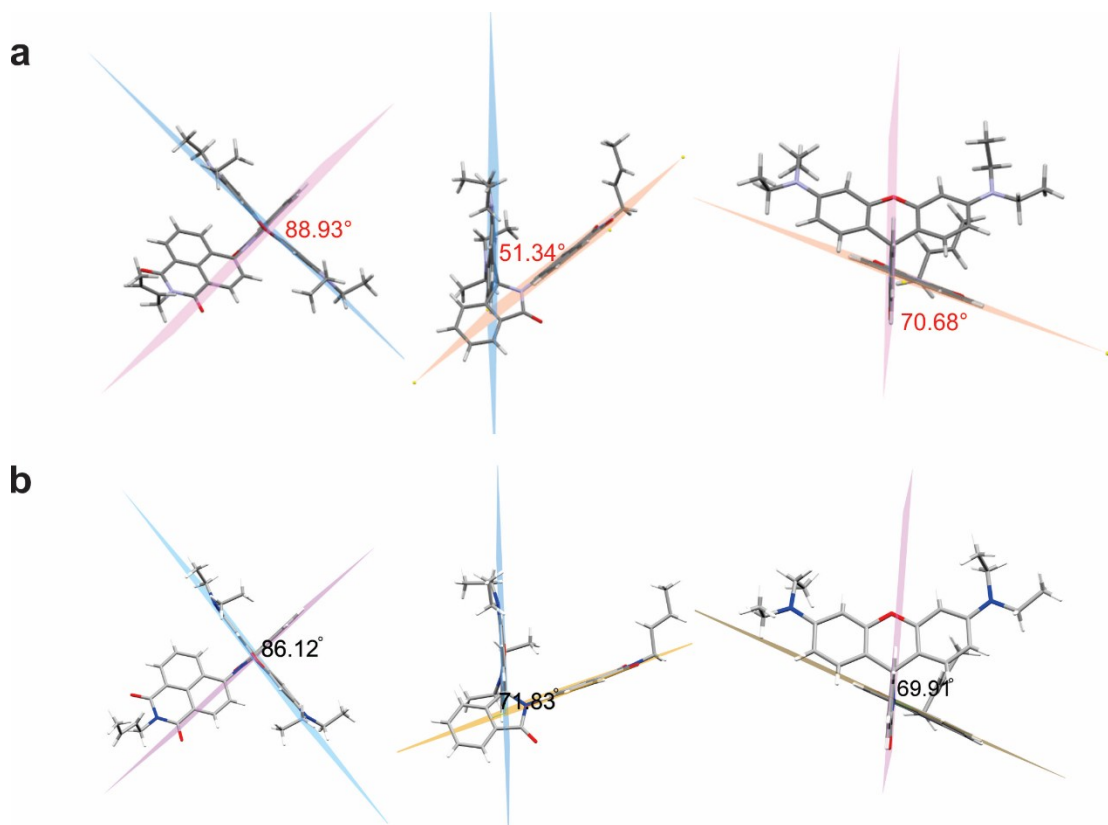


Figure S9. Dihedral angles between xanthene, naphthalimide and isoindolin-1-one moieties in (a) the **RhB-Naph** monomer (from DFT calculations) and (b) dimer (extracted from the crystal structure).

11. Vertical excitation energies to various singlet excited states, optimized molecular structure, HOMO and LUMO and of Naph in dichloromethane.

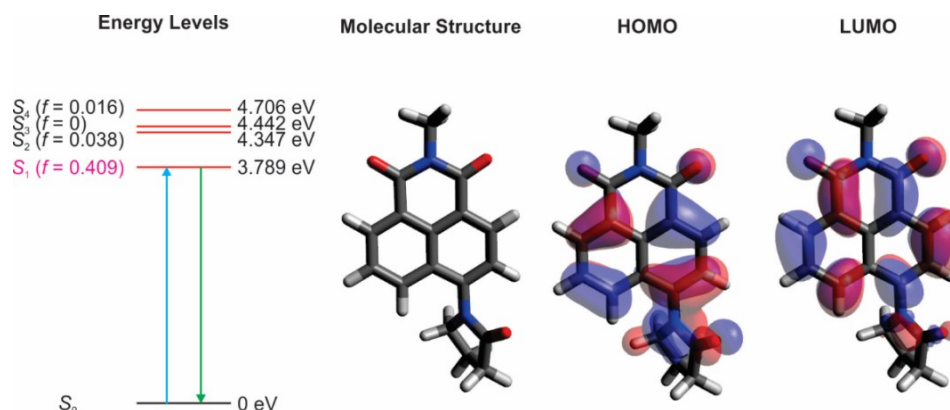


Figure S10. (a) Vertical excitation energies to various singlet excited states, optimized molecular structure, HOMO and LUMO and of **Naph** in dichloromethane.

12. Phosphorescence spectra of frozen solution of RhB-Naph (10^{-4} M, 77 K) in different solvent.

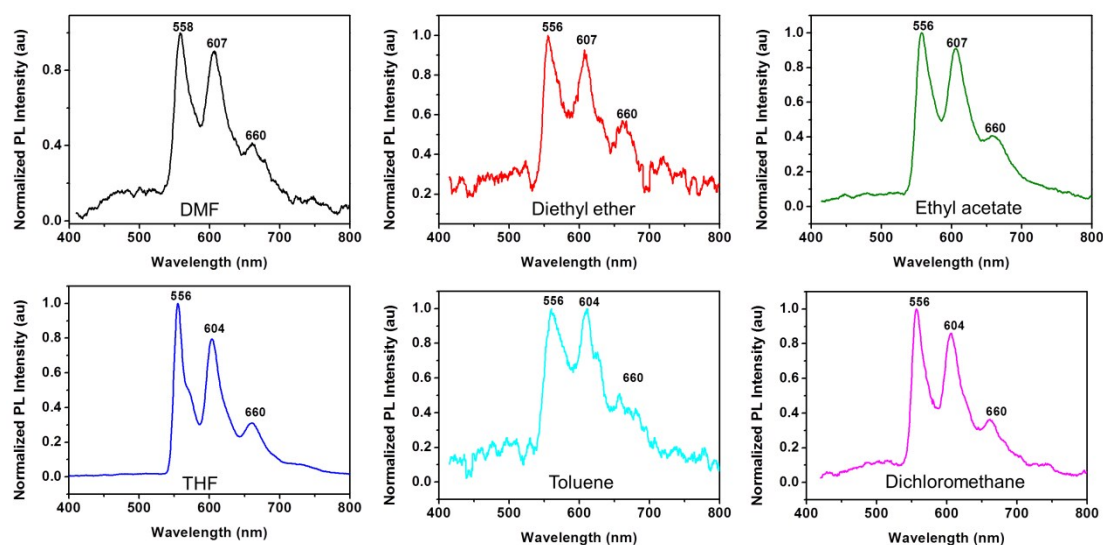


Figure S11. Phosphorescence spectra of frozen solution of **RhB-Naph** (10^{-4} M, 77 K) in different solvent after turning off the 365 nm excitation light immediately.

13. PXRD pattern of the pristine powder and the simulated PXRD pattern delineated on the basis of the crystal structure using the single crystal software Mercury 3.10.1.

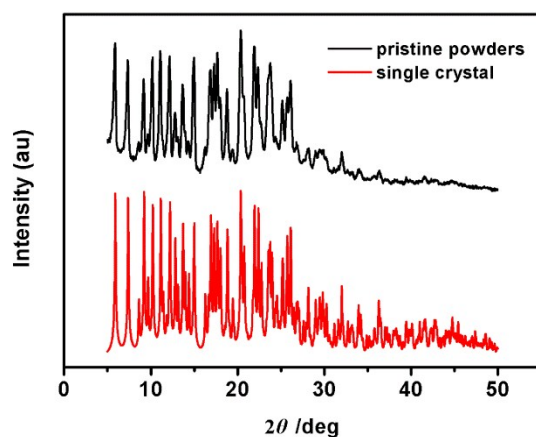


Figure S12. PXRD pattern of the pristine powder and the simulated PXRD pattern delineated on the basis of the crystal structure using the single crystal software Mercury 3.10.1.

Notes: The simulated PXRD pattern from the **RhB-Naph** crystal data was accorded well with the pattern of the pristine powder, suggesting that the pristine powder was mainly composed of the microcrystals of **RhB-Naph**.

14. Fluorescent lifetimes of RhB-Naph powders after different treatments.

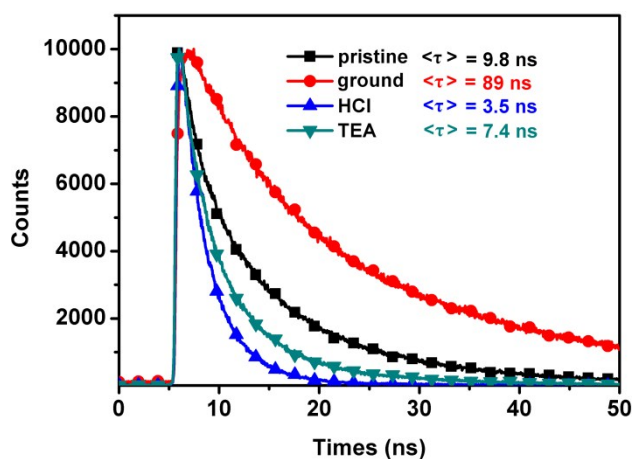
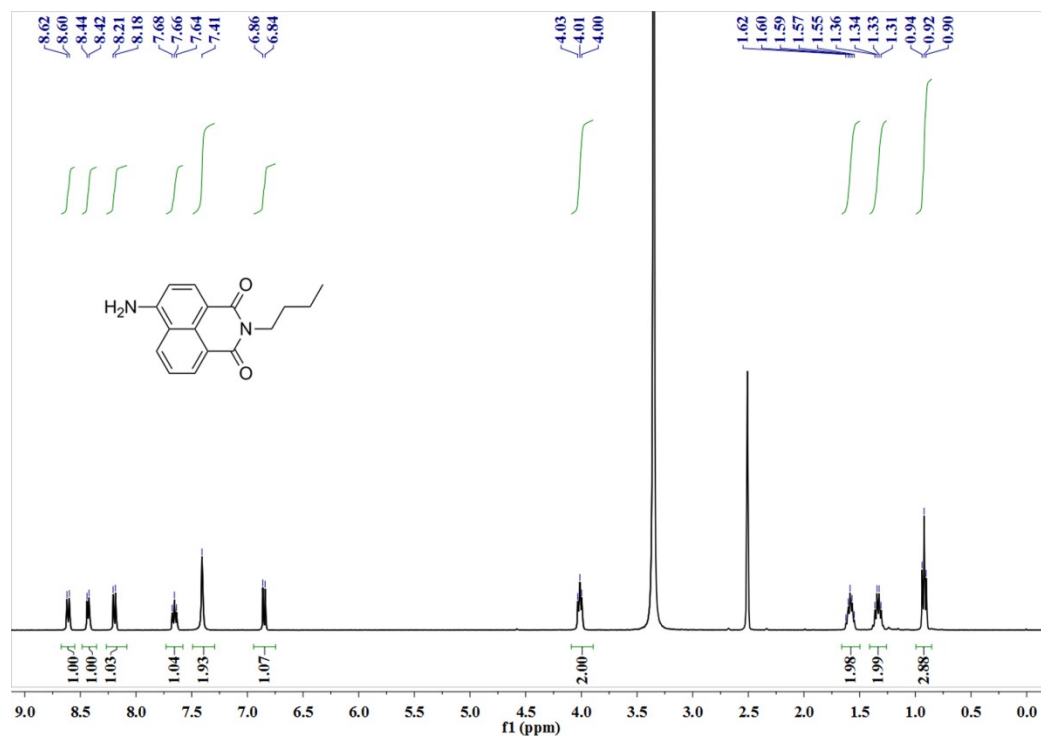


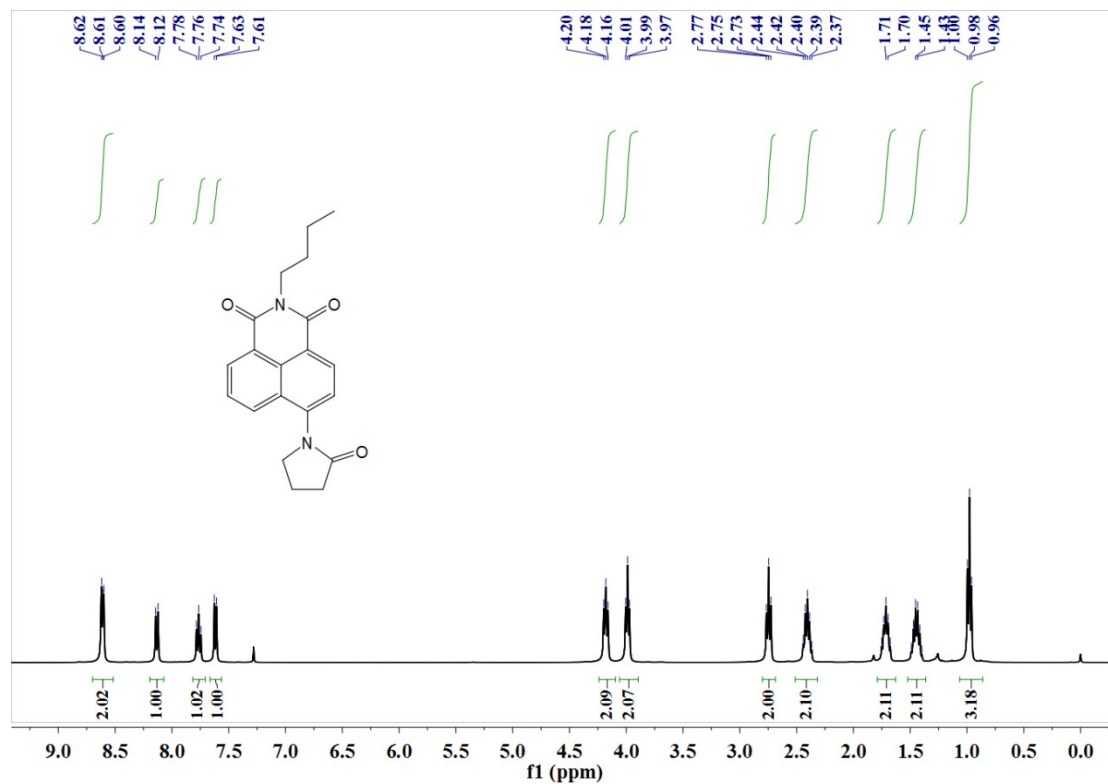
Figure S13. Fluorescent lifetimes of **RhB-Naph** powders after different treatments.

Notes: The emission lifetime of **RhB-Naph** powders have been measured under different treatments, including pristine powder (9.8 ns), grinding (89 ns), fuming with acid (3.5 ns), fuming with TEA (7.4 ns). See Figure S13.

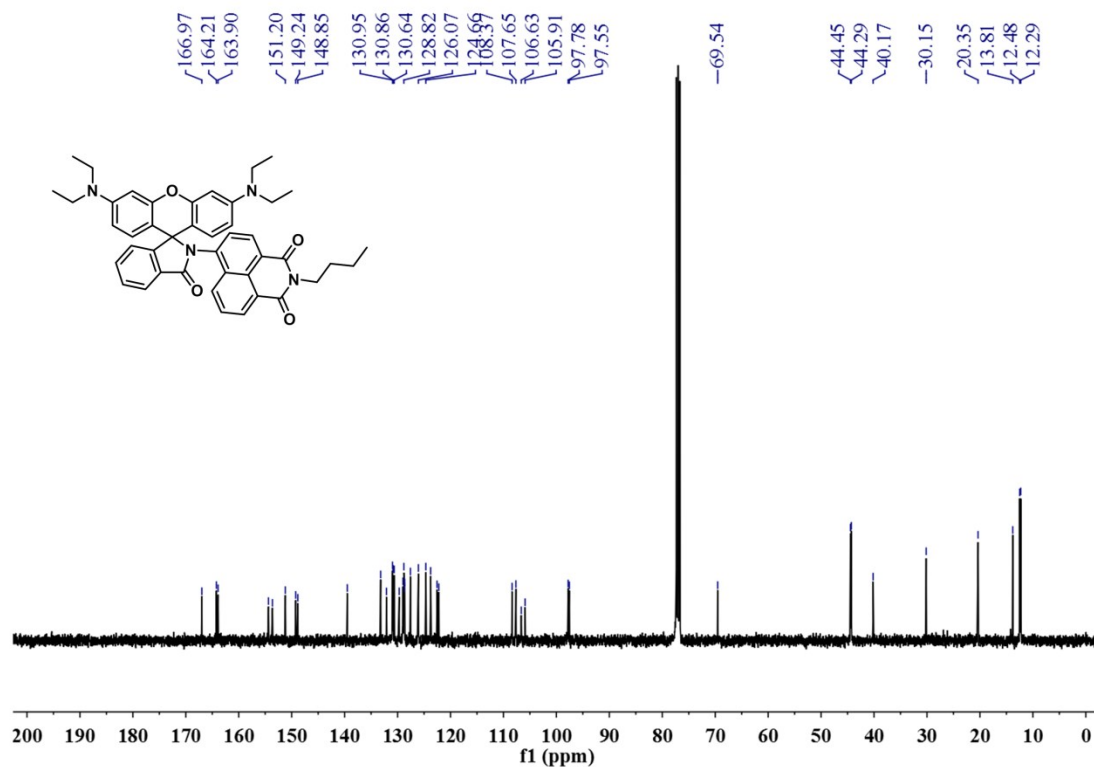
15. ^1H NMR, ^{13}C NMR and HRMS spectra of the compounds



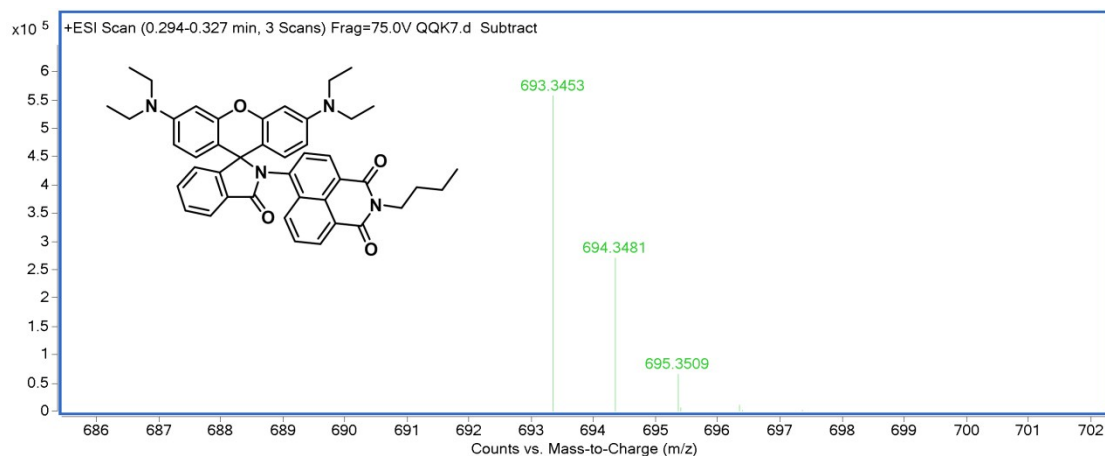
^1H NMR spectrum of 4-Amino-9-(*n*-butyl)-1,8-Naphthalimide in $\text{DMSO-}d_6$.



^1H NMR spectrum of Naph in CDCl_3 .



^{13}C NMR spectrum of **RhB-Naph** in CDCl_3 .



HRMS (ESI) of **RhB-Naph**.

16. References

1. K. Tsukamoto, S. Shimabukuro, M. Mabuchi and H. Maeda, *Chem. - Eur. J.*, 2016, **22**, 8579.
2. M. J. Frisch, G. W. Trucks, H. B. Schlegel, G. E. Scuseria, M. A. Robb and J. R. Cheeseman, *et al. Gaussian 16, Revision A. 03*, Gaussian, Inc., Wallingford, CT, 2016.
3. Y. Zhao and D. G. Truhlar, *Theor. Chem. Acc.*, 2008, **120**, 215.
4. A. V. Marenich, C. J. Cramer and D. G. Truhlar, *J. Phys. Chem. B*, 2009, **113**, 6378.
5. L. Palatinus and G. Chapuis, *J. Appl. Cryst.*, 2007, **40**, 786-790.
6. G. M. Sheldrick, *Acta Cryst.*, 2008, **A64**, 112-122.

7. O. V. Dolomanov, L. J. Bourhis, R. J. Gildea, J. A. K. Howard and H. J. Puschmann, *Appl. Cryst.*, 2009, **42**, 339.

8. W. C. Silvers, B. Prasai, D. H. Burk, M. L. Brown and R. L. McCarley, *J. Am. Chem. Soc.*, 2013, **135**, 309.